EurJIC European Journal of Inorganic Chemistry
ChemPubSoc Europe
FULL PAPER

DOI:10.1002/ejic.201500324

Benzoato and Thiobenzoato Ligands in the Synthesis of Dinuclear Palladium(III) and -(II) Compounds: Stability and Catalytic Applications

Francisco Estevan,[a] Susana Ibáñez,[a] Albert Ofori,[b] Pipsa Hirva,*[b] Mercedes Sanaú,[a] and Mª Angeles Úbeda*[a]

Keywords: Homogeneous catalysis / Electrochemistry / Palladium / S ligands / Structure elucidation / Density functional calculations

New palladium(III) compounds of formula $Pd_2[(C_6H_4)PPh_2]_2[OXC(C_6H_5)]_2Cl_2$ [**3a** (X = O); **3b** (X = S)] were obtained by the oxidation of the analogous palladium(II) ones with $PhICl_2$ and were characterized by ^{31}P, ^{1}H, and ^{13}C NMR spectroscopy at 223 K. Compound **3a** was also structurally characterized by single-crystal X-ray diffraction methods, which revealed a Pd–Pd distance of 2.5212(10) Å. DFT calculations were conducted to study the stability of all of these new palladium(III) and -(II) compounds with focus on the influence of the O↔S substitution of the donor atom in the ligand. The palladium(II) compounds $Pd_2[(C_6H_4)PPh_2]_2[OXC(C_6H_5)]_2$ [**2a** (X = O), **2b** (X = S)] were also tested as precatalyst in two reactions: (1) the acetoxylation of 2-phenylpyridine and (2) the room-temperature 2-phenylation of indoles. Compound **2b** is a better precatalyst than **2a** in the first reaction (4 h; isolated yield, 67.5 vs. 50.4 %). In the second catalytic reaction, isolated yields of 97 (10 h, substrate: 1-methylindole) and 99 % (24 h, substrate: indole) were obtained with **2a** as the precatalyst, whereas **2b** gave low or no conversion.

Introduction

Even though the chemistry of palladium(III) compounds has undergone some major advances in the last ten years, this area is still not well known.[1]

Few dinuclear palladium(III) compounds have been well characterized since the first one with a Pd_2^{6+} core and a M–M bond was synthesized by Cotton and co-workers.[2] In recent years, our research has focused on the chemistry of this type of palladium(III) compounds, and we reported the first high-yield syntheses of these complexes.[3]

Moreover, Ritter and co-workers have characterized not only other discrete dinuclear[4] and 1D wire[5] palladium(III) complexes with metal–metal bonds but also a transition-state analogue for the oxidation of a palladium(II) compound to a palladium(III) one.[6] Furthermore, Mirica and co-workers and Bauer and co-workers reported new dinuclear compounds with Pd^{III}–X–Pd^{III} bridges in their structures.[7]

We performed a topological charge-density analysis of several *ortho*-metalated palladium(III) compounds with bridging N,S-donor ligands, which had been synthesized and characterized previously.[3e] The results were compared with those obtained with similar compounds with N,O-donor ligands. The study showed that the contribution of the sulfur p orbitals to the highest occupied molecular orbital (HOMO) allows a greater stabilization of the dinuclear palladium(III) compounds. In this paper, we present the synthesis and characterization of new dinuclear palladium(III) compounds of formula $Pd_2[(C_6H_4)PPh_2]_2[OXC(C_6H_5)]_2Cl_2$ (X = O or S; Figure 1, A) obtained by the oxidation of compounds of type B (Figure 1, B). The target is the study of their reactivity and stability to obtain information about how these compounds are affected by changes of the O donor atom of the bridging ligand to a softer atom such as S. DFT calculations have been performed for all of the palladium(III) and -(II) compounds, and the results have been compared with those for other carboxylate compounds.

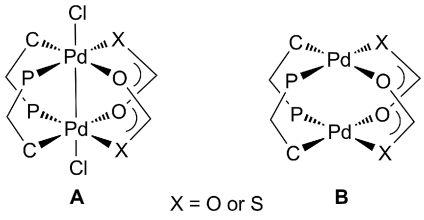

Figure 1. Dinuclear metalated (A) palladium(III) and (B) palladium(II) compounds.

Palladium compounds are effective catalysts in cross-coupling reactions. The catalytic direct oxidation of arene

[a] Departament de Química Inorgànica, Universitat de València, Dr. Moliner 50, 46100 Burjassot, València, Spain
E-mail: angeles.ubeda@uv.es
http://www.uv.es
[b] Department of Chemistry, University of Eastern Finland, Joensuu Campus, P. O. Box 111, 80101 Joensuu, Finland
E-mail: pipsa.hirva@uef.fi
http://www.uef.fi

Supporting information for this article is available on the WWW under http://dx.doi.org/10.1002/ejic.201500324.

C–H bonds has the potential to generate carbon–heteroatom or C–C bonds.[8] In this context, hypervalent iodine(III) compounds have found extensive applications as strong electrophiles and powerful oxidants.[9]

In recent years, the synthetic accessibility to palladium compounds in high oxidation states (III and IV) has changed the paradigm of some of these oxidation catalytic processes and allowed the development of new strategies in which these compounds are considered as intermediates. Sanford and Hickman described the relevance and the advantages of "high-valent" organometallic palladium(III) and -(IV) intermediates over the more common "low-valent" analogues.[10] Ritter and co-workers produced the first evidence of dinuclear palladium(III) intermediates in the Pd-catalyzed oxidative functionalization of C–H bonds.[11] Mirica and co-workers detected by UV/Vis spectroscopy the presence of dinuclear palladium(III) complexes with a halide bridging ligand in the Kharasch addition of polyhaloalkanes to alkenes.[12] Bauer and co-workers demonstrated that palladium(III) compounds act as enantioselective catalysts in the asymmetric rearrangement of allylic trifluoroacetimidates.[7b]

Sanford and co-workers described some interesting strategies for selectivity in the C–H bond functionalization that are based on the control of the substrate, the catalyst, or both.[13] The substrate control can be accomplished either through some coordinating functional groups that can direct the activation to a specific C–H bond (benzo[*h*]quinoline, 2-phenylpyridine) or through highly activated C–H sites (indoles and pyrroles), which allow the functionalization with high selectivity for one C–H bond in the molecule.

Considering these strategies for the control of the selectivity in catalyzed C–H bond functionalization and to study the different behavior of the dinuclear metalated palladium(II) compounds described in this paper, we have tested them in three catalytic direct C–H bond oxidation reactions: the acetoxylation of 2-phenylpyridine and the 2-phenylation of the 1-methylindole and indole. The results are compared with those published by Sanford and co-workers[14,15] and Ritter and co-workers.[4b,11a] Notably, these authors considered palladium(IV) or -(III) compounds as intermediates in these catalytic processes.

Results and Discussion

Dinuclear Palladium(II) Compounds with Benzoato and Thiobenzoato Bridging Ligands

Synthesis and Characterization

The reactions of $[Pd\{(C_6H_4)PPh_2\}Br]_4$ (**1**) with silver benzoate or thiobenzoate produced $Pd_2[(C_6H_4)PPh_2]_2[OXC(C_6H_5)]_2$ [**2a** (X = O), **2b** (X = S); Scheme 1].

The ^{31}P NMR spectra of **2a** and **2b** showed a single signal, and the chemical shifts are listed in Table 1. Owing to the asymmetric thiobenzoato ligand in **2b**, there are three possible isomers (Figure 2), but the ^{31}P NMR spectrum indicated that only one of the two possible isomers with magnetically equivalent phosphorus nuclei was the final product of the synthesis (Figure 2, C or D). The difference in the observed chemical shifts between **2a** and **2b** suggests that the atom *trans* to the phosphorus atom is different in both compounds.

Table 1. ^{31}P NMR spectroscopy data for palladium(II) and -(III) compounds.

Pd^{II} compounds	δ [ppm] 298 K	Pd^{III} compounds	δ [ppm] 223 K
2a	18.7	**3a**	–13.0
2b	13.8	**3b**	–16.9

Compounds **2a** and **2b** were structurally characterized by single-crystal X-ray diffraction methods. ORTEP views of both compounds are shown in Figure 3, and selected bond lengths and angles are given in Table 2.

Both complexes show a paddlewheel structure in which the dimetallic unit is supported by two *cisoid ortho*-met-

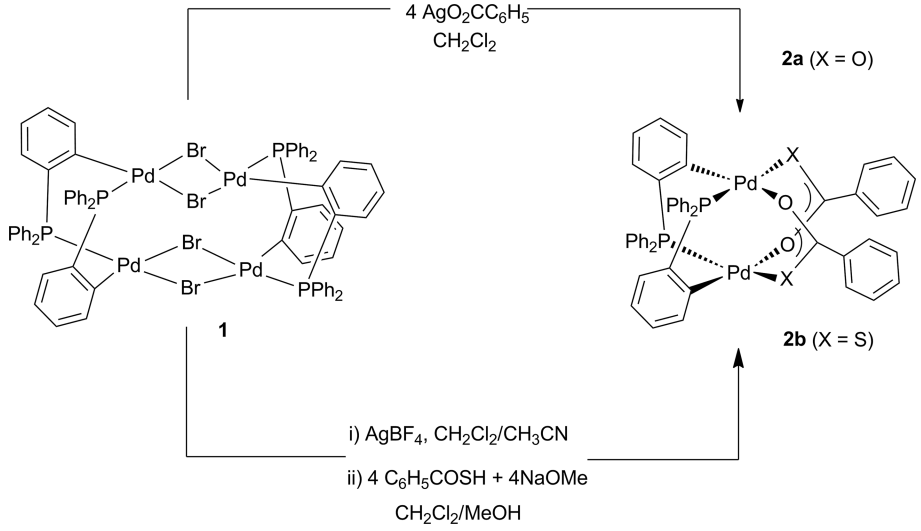

Scheme 1. Synthesis of **2a** and **2b** (isomer C).

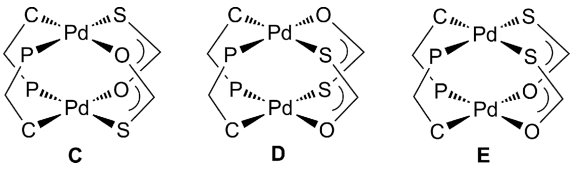

Figure 2. Isomers of **2b**.

Table 2. Selected distances [Å] and angles [°] for **2a** and **2b**.

	2a	**2b**
Pd1–Pd2	2.6865(10)	2.7395(4)
Pd1–P1	2.231(3)	2.2946(9)
Pd1–C_{met}	1.977(11)	1.984(4)
P1–Pd1–X_{trans}	172.1(2)	175.28(4)
C_{met}–Pd1–O_{trans}	173.7(4)	179.12(14)

alated phosphine ligands and two benzoato (**2a**) or two thiobenzoato (**2b**) ligands to complete the palladium square-planar coordination mode. The Pd–Pd distances of 2.6865(10) and 2.7395(4) Å are shorter than the sum of the van der Waals radii (3.26 Å). We have included a charge-density analysis at the Pd–Pd bond critical points (BCPs) that supports a $Pd^{II}\cdots Pd^{II}$ interaction with some electron sharing in both of the palladium(II) compounds, as was already observed for other dinuclear palladium(II) compounds.[3a,3c,3d,3f] This interaction was observed in the UV/Vis spectra, in which the lowest-energy signal involved mainly d–d excitations (Supporting Information, Figures S1 and S2).

A comparison with the Pd–Pd distances of previously structurally characterized carboxylate *ortho*-metalated dinuclear palladium(II) compounds[16] reveals that **2a** shows the second-shortest distance (Table 3) and the distance is larger in carboxylate compounds with electron-withdrawing groups. This trend is completely consistent with the computationally optimized Pd–Pd distances, which are longer for carboxylates with CF_3 and C_6F_5 groups than for **2a**.

Table 3. Pd–Pd distances in carboxylate dinuclear palladium(II) compounds.

R in $Pd_2[(C_6H_4)PPh_2]_2$-$[O_2CR]_2$	Experimental Pd–Pd distance [Å]	Computational Pd–Pd distance [Å]
CF_3	2.7229(8)[a]	2.727
$C(CH_3)_3$	2.6779(15)[a]	2.707
C_6F_5	2.7078(6)[a]	2.724
C_6H_5	2.6865(10)	2.710

[a] Ref.[16]

Compound **2b** shows a longer Pd–Pd distance of 2.7395(4) Å, and this value is in the range of those observed in other paddlewheel *ortho*-metalated palladium compounds with N,S-donor ligands (2.7212–2.8031 Å).[3e] The structure shows that only the symmetric isomer C with the O atom *trans* to the C atom and the S atom *trans* to the P atom was obtained, in agreement with the ^{31}P NMR spectrum. This structure explains the chemical shift differences observed in the ^{31}P NMR spectra of **2a** and **2b**. The preference for isomer C was also confirmed computationally, as isomer C had a lower total energy relative to the other symmetric isomer D by ca. 32 kJ mol^{-1}.

Electrochemical Studies

The electrochemical behavior of **2a** and **2b** has been investigated to evaluate them as precursors in the synthesis of new palladium(III) complexes. The electrochemical oxidation of both complexes was conducted in CH_3CN at room temperature, and the cyclic voltammograms are shown in Figure 4.

Compound **2a** showed similar electrochemical behavior to that of other carboxylate dinuclear palladium(II) compounds previously described.[16] In the initial anodic scan, two reversible waves were observed at potential values of 0.92 and 1.20 V. The first wave can be described in terms of a reversible one-electron transfer process in the starting Pd_2^{4+} complexes to yield the mixed-valent Pd_2^{5+} cationic species. The electrochemical potential of this wave is 0.92 V versus Ag/AgCl(satd. KCl), and has been calculated as the half-sum of the anodic and cathodic peak potentials. As the

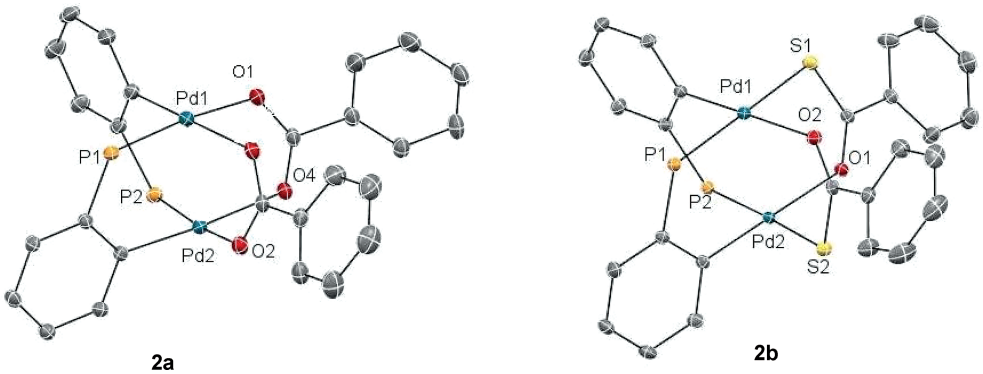

Figure 3. ORTEP views of **2a** and **2b** with the H atoms and the nonmetalated phenyl groups of the phosphines omitted for clarity. Ellipsoids drawn at 15% probability.

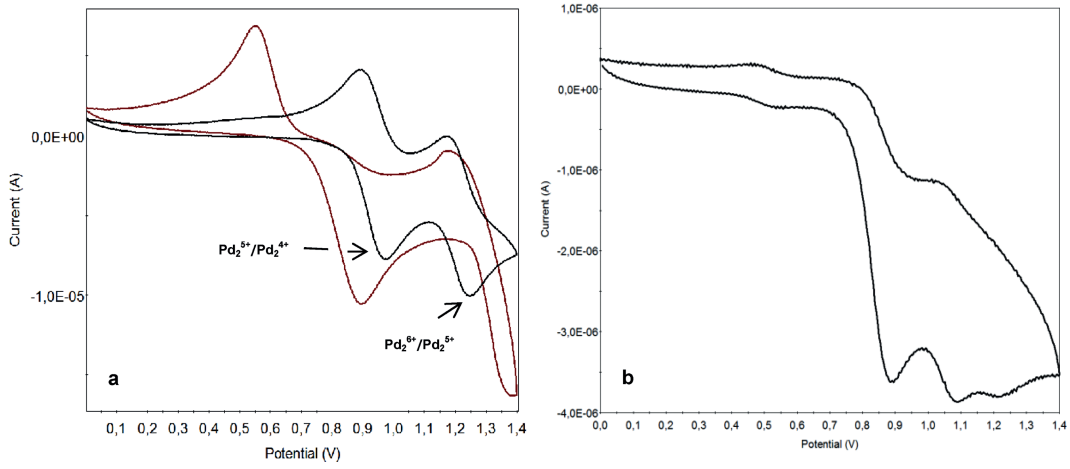

Figure 4. Cyclic voltammograms for (a, – black) **2a**, (a, – red) **2a** in presence of TEACl, and (b) **2b**.

potential value decreases with the electron-donating ability of the carboxylato ligand,[16] this value is lower than those for complexes that contain carboxylates with electron-withdrawing groups such as CF_3 or C_6F_5 (Table 4).

Table 4. Summary of electrochemical data for carboxylate dinuclear palladium(II) complexes.

R in $Pd_2[(C_6H_4)PPh_2]_2[O_2CR]_2$	$E_{1/2}^{ox1}$ [V]	$E_{1/2}^{ox2}$ [V]
CH_3	0.96[a]	1.38[a]
CF_3	1.25[a]	1.49[a]
$C(CH_3)_3$	0.84[a]	1.31[a]
C_6F_5	1.04[a]	1.35[a]
C_6H_5	0.92	1.20

[a] Electrochemical oxidation was conducted in CH_2Cl_2. No appreciable differences in the electrochemical potential values were observed in the electrochemical oxidation of ferrocene conducted in CH_2Cl_2 or CH_3CN.[16]

The second reversible wave at an electrochemical potential of 1.21 V was assigned to the $Pd_2^{5+} \rightarrow Pd_2^{6+}$ process.

Compound **2b** showed an irreversible oxidation wave at 0.89 V, and the reduction wave at 0.81 V could be seen only at high scan rates (0.40 $V s^{-1}$). A second oxidation process, also irreversible, was observed at 1.09 V and, as for the above process, the corresponding reduction wave was observed at high speeds at 1.02 V. These potentials are lower than those observed for **2a** and show the higher electron-donating capacity of the thiobenzoato ligand relative to the benzoato ligand.

Cyclic voltammograms for both compounds were also recorded in the presence of two moles of chloride ions from tetraethylammonium chloride (TEACl) per mole of the dinuclear palladium(II) compound. The aim was to study how the presence of ligands that can occupy the axial position influences the stability of the species formed in the electrochemical oxidation.

For **2a**, the voltammogram of which showed two reversible waves, the addition of chloride ions changed the electrochemical behavior. The voltammogram showed one single oxidation anodic wave at a potential slightly lower than the first one recorded (Figure 4, a, red). This wave approaches an irreversible two-electron oxidation process followed by a reduction wave at 0.57 V in a subsequent cathodic scan. This electrochemical process involves a two-electron oxidation with the addition of two chloride ions to afford a $Cl–Pd^{III}–Pd^{III}–Cl$ species. The voltammogram of the palladium(III) compound **3a** (Figure S3) showed the same anodic wave and, therefore, supports the formation of this compound through the electrochemical oxidation of **2a** in the presence of chloride ions. This behavior was observed previously and implies that the oxidation of the dinuclear palladium(II) compounds is followed by the addition of a chloride ion in the axial position.[3f,16,17]

The voltammogram of **2b** in the presence of two moles of chloride ions (TEACl) was similar to that observed for **2a** under the same conditions. A first oxidation wave, also irreversible, appeared at lower potentials (0.78 V). The second oxidation wave at 1.3 V can be assigned to the oxidation of the chloride. In the cathodic scan, a new irreversible wave was observed at 0.38 V (Figure S4).

Dinuclear Palladium(III) Compounds with Benzoato and Thiobenzoato Bridging Ligands

The reversible electrochemical behavior observed for the Pd_2^{5+}/Pd_2^{4+} and Pd_2^{6+}/Pd_2^{5+} processes in **2a** suggested that it is a suitable starting complex for the synthesis of the palladium(III) counterpart. Despite the irreversible electrochemical behavior for **2b**, DFT calculations have confirmed that the formation of Pd–Cl bonds through the chemical oxidation of palladium(II) compounds with $PhICl_2$ can stabilize the obtained palladium(III) compounds.[3d,3e] With this observation in mind, the syntheses of new palladium(III) compounds by chemical oxidation have been addressed.

Chemical Oxidation of 2a and 2b

The oxidation of **2a** and **2b** with $PhICl_2$ allowed us to obtain dinuclear Pd^{III} compounds of formula $Pd_2[(C_6H_4)PPh_2]_2[OXC(C_6H_5)]_2Cl_2$ [**3a** (X = O), **3b** (X = S); Scheme 2].

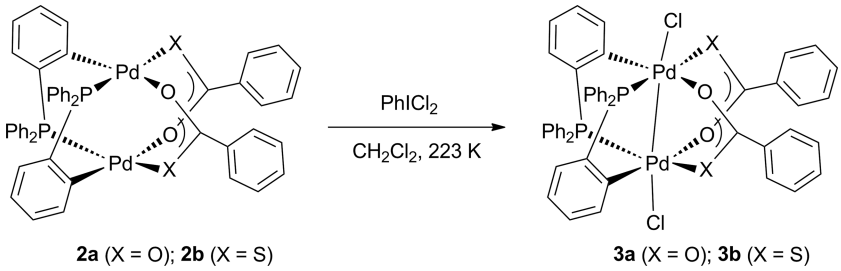

Scheme 2. Synthesis of **3a** and **3b**.

The reactions were followed by ^{31}P NMR spectroscopy from 200 to 298 K, which showed the stability of these compounds. The ^{31}P NMR spectra of both compounds showed only a single signal that is shifted toward high field by ca. 30 ppm relative to the observed signals for **2a** and **2b** (Table 1). In agreement with previous reports, this indicates the formation of palladium(III) compounds.[3]

Compounds **3a** and **3b** were relatively stable at room temperature and they were synthesized and characterized by ^{13}C, ^{1}H, and ^{31}P NMR spectroscopy at low temperature (223 K).

Compound **3a** was also structurally characterized by single-crystal X-ray diffraction methods. The structure is shown in Figure 5 together with important bond lengths and angles.

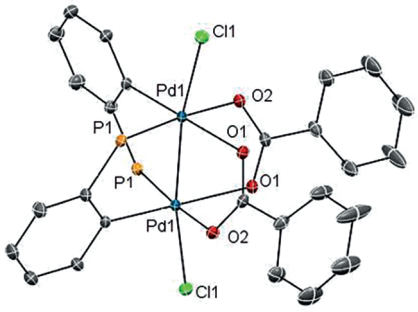

Figure 5. ORTEP view for **3a** with the H atoms and the non-metalated phenyl groups of the phosphines omitted for clarity. Ellipsoids drawn at 25% probability. Important bond lengths [Å] and angles [°]: Pd1–Pd1 2.5212(10), Pd1–P1 2.2521(14), Pd1–C_{met} 2.033(5), P1–Pd1–X_{trans}, 176.28(18), C_{met}–Pd1–O_{trans}, 174.88(10).

The Pd_2^{6+} unit is bridged by two *cisoid ortho*-metalated phosphine ligands and two benzoato ligands in a head-to-tail arrangement. Two chlorido ligands are coordinated in axial positions. The Pd–Pd distance of 2.5212(10) Å is one of the shortest among the characterized paddlewheel *ortho*-metalated palladium(III) derivatives (Table 5) and all of the discrete dinuclear palladium(III) compounds described in the literature.[2–4]

Unfortunately, suitable crystals of **3b** for X-ray diffraction methods could not be obtained.

Table 5. Pd–Pd distances in carboxylate dinuclear palladium(III) compounds.

R in $Pd_2[(C_6H_4)PPh_2]_2$-$[O_2CR]_2Cl_2$	Experimental Pd–Pd distance [Å]	Computational Pd–Pd distance [Å]
CH_3	2.5294(17)[a]	2.548
CF_3	2.5434(4)[a]	2.566
$C(CH_3)_3$	2.5241(9)[a]	2.550
C_6H_5	2.5212(10)	2.553

[a] Ref.[3b]

DFT Studies of Pd^{II} and Pd^{III} Compounds

All of the Pd^{II} and Pd^{III} compounds were computationally fully optimized at the DFT level of theory, and the nature of the bonding interactions was studied by using the Quantum Theory of Atoms in Molecules (QTAIM). In particular, we wanted to observe how the replacement of the hard oxygen atom in the carboxylato ligands with the softer sulfur atom in the thiocarboxylato ones would affect the nature of the interactions. The optimized structures are presented in Figure 6 along with selected distances. A comparison of the properties of the electron density at the BCPs is provided in Table 6.

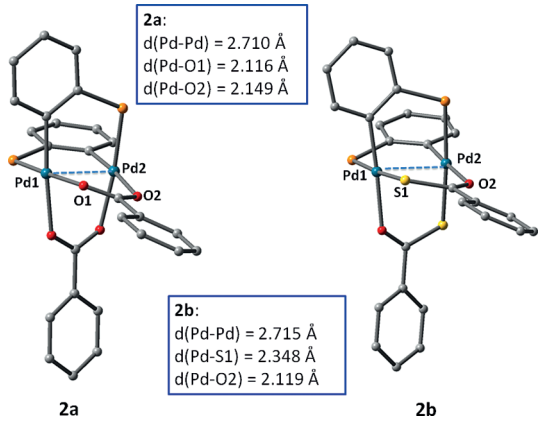

Figure 6. Optimized structures of the Pd^{II} carboxylate and thiocarboxylate complexes **2a** and **2b**. For clarity, hydrogen atoms and free phenyl groups of the phosphine ligands are omitted. Color scheme: Pd green, O red, S yellow, P orange, C gray. The blue dashed lines depict the axial Pd–Pd interactions. The Pd–Pd and Pd–X distances are shown in the boxes.

The atom *trans* to the phosphorus atom has the only major effect on the geometry and properties of the Pd^{II} compounds with either O,O or O,S ligands. The *trans* effect shortens the Pd–O distance notably in the carboxylate complex **2a**, which leads to stronger bonding interactions (–144 vs. –128 kJ mol^{-1}) as well as more electron density at the bond critical points for the oxygen atoms *trans* to the P atom (Figure 6 and Table 6). However, in **2b** the increased

Table 6. Pd–Pd and Pd–X (X = S or O) distances [Å], electron density ρ [e Å^{-3}], and interaction energy E_{int} [kJ mol^{-1}] at the Pd–Pd and Pd–X BCPs in carboxylate and thiocarboxylate dinuclear palladium(II) compounds **2a** and **2b** and Pd^{III} compounds **3a** and **3b**. $|V|/G$ = ratio between potential energy density and kinetic energy density, Ω = delocalization index.

	2a (X = O)	**2b** (X = S)	**3a** (X = O)	**3b** (X = S)
d(Pd–Pd)	2.710	2.715	2.553	2.596
d(Pd–O2)[a]	2.149	2.119	2.142	2.168
d(Pd–X)	2.116	2.348	2.101	2.387
ρ(Pd–Pd)	0.301	0.277	0.447	0.417
ρ(Pd–O2)	0.466	0.427	0.491	0.511
ρ(Pd–X)	0.521	0.547	0.549	0.492
E_{int}(Pd–Pd)	–64	–57	–78	–70
E_{int}(Pd–O2)	–128	–118	–131	–138
E_{int}(Pd–X)	–144	–114	–149	–96
$\|V\|/G$ (Pd–Pd)	1.23	1.23	1.44	1.44
$\|V\|/G$ (Pd–O2)	1.01	0.99	1.02	1.02
$\|V\|/G$ (Pd–X)	1.03	1.32	1.04	1.32
Ω (Pd–Pd)	0.35	0.34	0.62	0.62
Ω (Pd–O2)	0.46	0.42	0.46	0.47
Ω (Pd–X)	0.49	0.74	0.50	0.65

[a] O2 is the oxygen atom *trans* to the *ortho*-metalated C atom, see Figure 6.

electron density at the Pd–S BCP does not lead to stronger metal–ligand bonding, as can be seen in the slightly lower interaction energies at the Pd–Pd, Pd–O2, and Pd–X bond critical points for the thiobenzoato compound. The weaker metal–ligand interactions suggest somewhat smaller stability for the thiocarboxylate compounds. On the other hand, the nature of the Pd–S bond is different from that of the Pd–O bond, and both the $|V|$/G values and the delocalization index (which gives an estimate of the bond index) predict more-covalent bonding for the Pd–S bonds than for the Pd–O bonds. A reason for the larger amount of electron sharing can be seen in the larger p-orbital contribution of the sulfur atoms in the HOMOs and lowest unoccupied molecular orbitals (LUMOs) of the molecules (Figure S2). The more-covalent nature of the Pd–S interaction is also observed in the Laplacian of the electron density (the second derivative of ρ), which is compared in Figure 7 for **2a** and **2b**. The Laplacian presentation also shows an additional interaction between sulfur atom S1 and one of the hydrogen atoms from the phenyl substituent of the thiobenzoato ligand. This weak hydrogen-bonding interaction (E_{int} = –11 kJ mol^{-1}) stabilizes the structure further and, hence, the overall stabilities of **2a** and **2b** are very similar.

The addition of two axial chlorido ligands to **2a** and **2b** showed that both compounds were readily oxidized to yield **3a** and **3b**. The stability of the oxidized compounds was studied by calculating the reaction energies of the model reaction $Pd_2[(C_6H_4)PPh_2]_2[OXC(C_6H_5)]_2 + Cl_2 \rightarrow Pd_2[(C_6H_4)PPh_2]_2[OXC(C_6H_5)]_2Cl_2$. The reaction energies were again similar at –146 and –140 kJ mol^{-1} for the O,O and O,S complexes, respectively, but somewhat larger than the previously reported reaction energies for N–N–N (triazenide)[3f] and N–C–N (amidinate)[3c] compounds, which gave energies of ca. –85 kJ mol^{-1}. However, the less-favorable oxidation of the triazenides and the benzamidinates

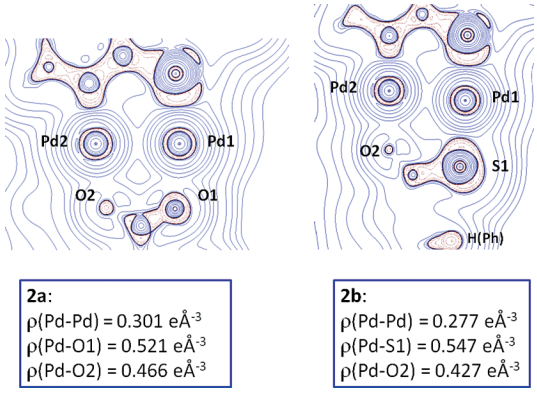

Figure 7. Laplacian of the electron density at the Pd1–Pd2–X plane (X = O or S) for **2a** and **2b**. The boxes show the electron-density values at the corresponding BCPs.

can be explained by steric reasons, as both ligands had bulky phenyl groups attached to the nitrogen atoms, which partially hindered the axial interaction of the chlorido ligands.

A closer inspection of the nature of the bonding interactions was done with the QTAIM method. The properties of the electron density for **3a** and **3b** are listed in Table 6 together with those of the corresponding Pd^{II} complexes.

The nature of the Pd–Pd interaction changes with the attachment of the axial chlorido ligands in the Pd^{III} compounds. The negative chlorido ligands donate electron density, which is mainly distributed to the metal atoms, and ρ increases notably at the Pd–Pd BCP. This leads to increased covalency and a stronger metal–metal interaction in both **3a** and **3b**. The metal–ligand bonding is also somewhat affected; in the carboxylate compound **3a**, the Pd–O interactions show increasing strength, but the opposite is true for **3b**: the Pd–S interaction has less electron density and smaller interaction energy in **3b** than in the parent **2b**. Thus, the axial interaction with the chlorido ligands strengthens the Pd–O interaction (in both **3a** and **3b**) but weakens the Pd–S interaction. However, again the sulfur atom of the thiobenzoato ligand is able to form an additional stabilizing S···H interaction with the phenyl group and, therefore, the stabilities of **3a** and **3b** are similar.

A comparison of the nature of the interactions in other carboxylate and thiocarboxylate compounds revealed only minor differences (Tables S1 and S2). Strongly electron-withdrawing substituents, such as CF_3, yield slightly less electron density at the Pd–Pd BCPs, which in turn weakens the interaction in both the Pd^{II} and the Pd^{III} compounds. This effect is also seen in larger Pd–Pd distances for R = CF_3.

Metalated Palladium(II) Compounds in the Catalytic Direct Oxidation of Arene C–H Bonds

Compounds **2a** and **2b** have been tested as precatalysts in oxidative C–H coupling reactions. To achieve site selectivity in the C–H bond functionalization, we have consid-

ered the strategies based on the substrate control reported by Sanford and co-workers.[13] 2-Phenylpyridine, the coordinating N atom of which can direct the C–H activation, and 1-methylindole or indole with highly activated C–H bonds have been used as substrates in the catalytic reactions.

Acetoxylation of 2-Phenylpyridine

The catalyzed C–H acetoxylation of 2-phenylpyridine to give **5** has been studied with iodobenzene acetate as the oxidant and **2a** and **2b** as precatalysts (Scheme 3). Different solvents, temperatures, and reaction times were tested, and the results are listed in Table 7.

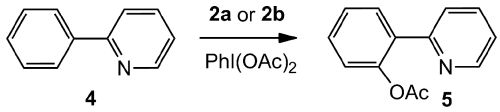

Scheme 3. Acetoxylation of 2-phenylpyridine.

Table 7. Acetoxylation of 2-phenylpyridine.

Entry	Solvent	Temp. [°C]	Time [h]	Isolated yield [%]	
				2a	**2b**
1	toluene/EtOAc (1:1)	80	2	15	44
2	toluene/EtOAc (1:1)	80	4	50	68
3	CH_3CO_2H	115	4	30	50
4	CH_3CN	80	4	38	57
5	EtOAc	50	20	8	9
6	EtOAc	60	8	11	12
7	EtOAc	80	5	28	34

The temperature plays an important role in this catalytic process. If the reaction is performed in ethyl acetate, the yields increase as the temperature increases, even if the reaction time decreases (Table 7, Entries 5–7). A 1:1 toluene/EtOAc mixture gave the best results among the solvents that were tested (Table 7, Entry 2). In all cases, **2b** was a better precatalyst than **2a**. All of the reactions were followed by ^{1}H NMR spectroscopy.

Without the presence of the palladium complexes, the reaction did not proceed.

Sanford, who pioneered this type of catalytic C–H oxidation reaction, obtained a yield of 52% for **5** after 12 h of reaction with CH_3CN as the solvent at 100 °C and $Pd(OAc)_2$ as the precatalyst.[14] With other 2-phenylpyridines with substituted phenyl groups as substrates, the yields for the acetoxylated product were generally higher.[18]

Subsequently, for the reaction in acetic acid at 80 °C and $Pd(OAc)_2$ as the precatalyst, Ritter and co-workers achieved yields of 15–37% after 12 h, depending on the amount of palladium compound used (see Supporting Information for ref.[4b]). The studies conducted by these researchers disclosed the first evidence of a dinuclear palladium(III) complex as an intermediate in the catalyzed C–H acetoxylation. The palladium(III) compound $Pd_2(2\text{-Phpy})_2(OAc)_2Cl_2$ (2-Phpy = 2-phenylpyridinate) in the presence of 20 equiv. of **4** at 40 °C gave **5** in 91% yield; therefore, this palladium(III) compound is a kinetically competent catalyst for the 2-phenylpyridine acetoxylation.[4b,11a]

2-Phenylation of 1-Methylindole and Indole

Compounds **2a** and **2b** have been tested as precatalysts in the room-temperature direct 2-phenylation of indoles (**6a** and **6b**) with $[Ph_2I]PF_6$ in acetic acid to give compounds **8a** and **8b**, respectively (Scheme 4). The reactions were followed by ^{1}H NMR spectroscopy, and the results are displayed in Table 8.

Table 8. 2-Phenylation of 1-methylindole (**6a**) or indole (**6b**).

Entry	Palladium compound	Substrate	Time [h]	Product	Isolated yield [%]
1	**2a**	**6a**	10	**8a**	97
2	$Pd_2[(C_6H_4)PPh_2]_2[O_2CCH_3]_2$	**6a**	9	**8a**	95
3	$Pd_2[(C_6H_4)PPh_2]_2[O_2CCF_3]_2$	**6a**	11	**8a**	90
4	**2a**	**6b**	24	**8b**	99
5	$Pd_2[(C_6H_4)PPh_2]_2[O_2CCH_3]_2$	**6b**	21	**8b**	98
6	$Pd_2[(C_6H_4)PPh_2]_2[O_2CCF_3]_2$	**6b**	36	**8b**	98

Compound **2a** is an efficient precatalyst for the direct phenylation of both indoles to give high isolated yields for **8a** and **8b**, but the reaction with 1-methylindole proceeded in a shorter reaction time (Table 8, Entries 1 and 4). The results were compared with those obtained with other carboxylate palladium compounds, and similar trends, that is, high isolated yields with similar reaction times for each substrate (Table 8, Entries 2, 3, 5, and 6), were obtained.

With **2b** as the precatalyst, the 1-methylindole phenylation proceeded less than 50% after 7 d of reaction, as observed by ^{1}H NMR spectroscopy. For indole, no 2-phenylindole was observed after 20 d of reaction, but only 50% of the initial indole remained in solution; therefore, some of the substrate evolved to unidentified products.

Other dinuclear palladium compounds have been applied in these catalytic reactions. We point out that the phenolate palladium derivative $Pd_2[(C_6H_4)PPh_2]_2[C_6H_5OC(O)CH_3]_2$ gave an isolated yield of **8a** of 93% with a reaction time of 2 h,[3d] and **8b** was obtained in 88% yield after 7 h with the triazenide palladium compound $Pd_2[(C_6H_4)PPh_2]_2[C_6H_5N{-}N{-}NC_6H_5]_2$ as the precatalyst.[3f] With the mononuclear palladium compound $IMesPd(OAc)_2$ [IMes = 1,3-bis(2,4,6-trimethylphenyl)imidazol-2-ylidene] as a potential catalyst and $[Ph_2I]BF_4$ as the oxidant, Sanford and co-workers ob-

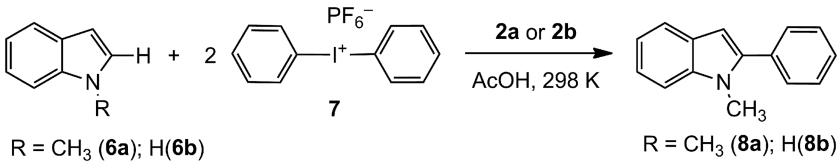

Scheme 4. 2-Phenylation of 1-methylindole (**6a**) and indole (**6b**).

tained an isolated yield of 86% of **8a** after 18 h of reaction and 81% of **8b** after 15 h.[15]

If the reaction was attempted without the presence of palladium complexes, compounds **8a** or **8b** were not observed. At the end of each reaction, a solid was obtained. These solids did not catalyze the phenylation reaction.

The HPF_6 obtained by the reaction of $[Ph_2I]PF_6$ with acetic acid decomposed at room temperature to give HF.[19]

With **3a** as the precatalyst, the 2-phenylation of 1-methylindole progressed less than 5% after 14 h. No reaction was observed with **3b**.

Mechanistic Insights from DFT Calculations

Previously, we established that the initial step in the 2-phenylation of 1-methylindole with palladium triazenides as precatalysts involved the axial attachment of a phenyl group to the palladium atom.[3f] In the present work, we repeated the computational procedure for **2a** and **2b** to check how probable the same initial step would be. The complexes optimized for the study are shown in Figure 8 with a comparison of the most important interactions. Selected geometrical and electronic parameters for the Pd^{III} carboxylate and thiocarboxylate compounds with axial phenyl groups are listed in Table S3. The nature of the bonding in the precatalysts **2a**, **2b**, **3a**, and **3b** is compared in Table 6.

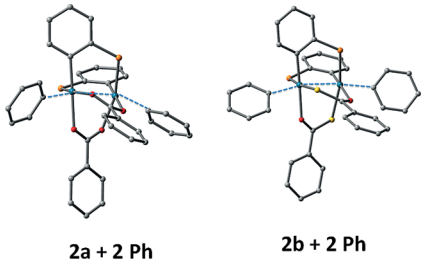

Figure 8. Optimized structures of the carboxylate and thiocarboxylate complexes with axial phenyl groups. For clarity, hydrogen atoms and free phenyl groups of the phosphine ligands are omitted. Color scheme: Pd green, O red, S yellow, P orange, C gray. The blue dashed lines depict the axial interactions.

The steric properties of **2a** and **2b** are rather different from those of the previously studied triazenides. Therefore, the axial sites are more open for the attachment of the phenyl rings, and the reactions are very favorable for the carboxylate and thiocarboxylate compounds. The relative reaction energies for the addition of two Ph^- groups to **2a** and **2b** showed that stable structures are formed (E_{react} = –40 and –68 kJ mol^{-1} for **2a** and **2b**, respectively). On the other hand, both **2a** and **2b** showed very similar properties for the Pd–C(Ph) interaction (Table S3), and it could be concluded that the first step of the catalysis reaction most probably would include the attachment of the phenyl ring to the palladium atoms at the axial site. When inspecting the effect of the axial phenyl groups on the nature of the Pd–Pd interaction, we noted that the originally antibonding HOMOs of **2a** and **2b** changed to bonding interactions involving the metal d orbitals (Figures S2 and S5). This change in the nature of HOMO led to the destabilization of the HOMO energy, as can be seen in Table S4. The LUMOs of (**2a** + 2Ph) and (**2b** + 2Ph) also concentrated at the axial direction, but in this case the contribution of the axial phenyl groups led to lower energy. On the other hand, the HOMO–LUMO gap was in the same range for **3a** and **3b**, which indicates a similar stability for the complexes with axial phenyl groups. However, no major differences could be found between complexes **2a** and **2b**, which would explain why the catalysis reaction would not proceed effectively with the O,S compound. In this case, it can be suggested that the difference comes from kinetic control rather than thermodynamic control.

Conclusions

The new palladium(III) compounds $Pd_2[(C_6H_4)PPh_2]_2[OXC(C_6H_5)]_2Cl_2$ [**3a** (X = O), **3b** (X = S)] are relatively stable at room temperature and have been synthesized and characterized by spectroscopic techniques at 223 K. Compound **3a** was also characterized by single-crystal X-ray diffraction methods, which revealed a Pd–Pd distance of 2.5212(10) Å.

DFT calculations have been conducted to study the stability of all of these new palladium(II) (**2a** and **2b**) and -(III) (**3a** and **3b**) compounds, and we focused on the influence of the O↔S substitution at the donor atom of the ligand. Although stronger Pd–O bonding interactions than Pd–S ones suggest a somewhat lower stability for **2b**, a weak interaction between the sulfur atom and one of the hydrogen atoms from the phenyl group of the thiobenzoato ligand stabilizes the structure; therefore, **2a** and **2b** have similar stabilities. In the oxidized compounds **3a** and **3b**, the axial chlorido ligands increase the covalency and strength of the metal–metal interaction in a similar way for both complexes, whereas the Pd–O interaction is strengthened, and the Pd–S interaction is weakened. Again, an additional sulfur–hydrogen interaction stabilizes **3b**.

The isolated palladium(II) compounds were tested as precatalyst in two reactions: (1) the acetoxylation of 2-phenylpyridine and (2) the room-temperature 2-phenylation of indoles. Compound **2b** is a better precatalyst for the first reaction (reaction time: 4 h; isolated yield: 67.5 vs. 50.4%). In the second catalytic reaction, isolated yields of 97 (reaction time: 10 h, substrate: 1-methylindole) and 99% (reaction time: 24 h, substrate: indole) were obtained with **2a** as precatalyst, whereas **2b** gave low or no conversion. DFT calculations were also performed to explore the potential Pd^{III}–Ph intermediates in the catalytic 2-phenylation of indoles. The study showed very similar properties for the Pd–C(Ph) interactions of both compounds.

Experimental Section

General: All of the reactions were performed under a dry nitrogen atmosphere by using Schlenk techniques. Solvents were purified according to standard procedures. Commercially available reagents were used as purchased. $[Pd((C_6H_4)PPh_2)Br]_4$,[20] **1**, and iodo-

benzene dichloride[21] were synthesized according to literature procedures. Solvent mixtures are v/v mixtures. Column chromatography was performed with silica gel (35–70 mesh).

NMR spectra were recorded with Bruker 400 and 500 AMX spectrometers with samples as solutions in deuterated chloroform or dichloromethane at 298 K and low temperature. The chemical shifts are reported in ppm with tetramethylsilane (TMS; ^{1}H and ^{13}C) and 85% H_3PO_4 (^{31}P) as references. The coupling constants (J) are in Hertz.

Elemental analysis was provided by SCSIE of the University of Valencia.

Suitable single crystals of **2a**, **2b**, and **3a**, were obtained by layering hexane over dichloromethane solutions of the corresponding compounds. The crystals were mounted on glass fibers, and the diffraction measurements were performed with a Nonius Kappa CCD area-detector diffractometer with Mo-K_α radiation (λ = 0.71073 Å). The structures were solved by direct methods and refined by least-squares techniques on weighted F^2 values for all reflections (SHELXTL, 6.14).[22] All non-hydrogen atoms were assigned anisotropic displacement parameters and refined without positional constraints. All hydrogen atoms except those bonded to oxygen atoms in water molecules, were calculated with a riding model. Crystals of **2a** and **3a** crystallized with disordered water molecules, which led to difficulties with modeling the solvent. In both cases, the H atoms corresponding to those water molecules could not be located from difference Fourier maps. Complex neutral-atom scattering factors were used.

CCDC-1052931 (for **2a**), -1052932 (for **2b**), and -1052933 (for **3a**) contain the supplementary crystallographic data for this paper. These data can be obtained free of charge from The Cambridge Crystallographic Data Centre via www.ccdc.cam.ac.uk/data_request/cif.

The electrochemical studies were performed at room temperature with a 273 A PAR potentiostat in a three-electrode cell. The working electrode was a Pt electrode with a surface of 3.1 mm^2, the counter electrode was a Pt wire, and the reference electrode was Ag/AgCl (saturated KCl). The solvent was CH_3CN/0.1 M Bu_4NPF_6, the concentration of the compounds in the solutions was 0.5 mM, and the scan rate was 50 $mV\,s^{-1}$. Under these conditions, E_a for the couple Fc/Fc^+ (Fc = ferrocene) was 0.55 V.

Silver Benzoate: In a 1:1 stoichiometric ratio, a solution of $AgNO_3$ (0.5 mmol) in water (1 mL) was added under vigorous stirring to a CH_2Cl_2 solution (2 mL) of benzoic acid (0.5 mmol) previously deprotonated with a methanolic solution of NaOMe. A white precipitate was collected by filtration, washed with MeOH (2 × 4 mL), and vacuum-dried. It was used without further purification, yield 617 mg (66%).

$Pd_2[(C_6H_4)PPh_2]_2[O_2CC_6H_5]_2$ (2a): $[Pd\{(C_6H_4)PPh_2\}Br]_4$ (**1**; 70 mg, 0.039 mmol) was suspended in CH_2Cl_2 (10 mL), and silver benzoate (40 mg, 0.175 mmol) was added. The reaction mixture was stirred for 24 h, after which the crude mixture was filtered through a short plug of Celite. The solution was evaporated to dryness, and the yellow solid precipitated by the addition of hexane was collected by filtration and washed with hexane, yield 73 mg (96%). ^{1}H NMR ($CDCl_3$, 500 MHz, 298 K): δ = 7.62 (m, 4 H, Ar), 7.45 (m, 2 H, Ar), 7.39 (m, 4 H, Ar), 7.24 (m, 2 H, Ar), 7.16 (m, 6 H, Ar), 7.07 (m, 6 H, Ar), 7.01 (m, 4 H, Ar), 6.87 (m, 4 H, Ar), 6.72 (m, 6 H, Ar) ppm. ^{31}P NMR ($CDCl_3$, 202 MHz, 298 K): δ = 18.7 (s) ppm. ^{13}C NMR ($CDCl_3$, 125 MHz, 298 K): δ = 175.1 (s, COO), 160.4 (t, $^{3}J_{P,C}$ = 11 Hz, C metalated), 139.8–122.0 (Ar) ppm. $C_{50}H_{38}O_4P_2Pd_2$ (977.60): calcd. C 61.43, H 3.92; found C 61.12, H 3.79.

X-ray Crystal Structure Data for 2a: Empirical formula $(C_{50}H_{38}O_4P_2Pd_2)_2{\cdot}5O(H_2)$, M_r = 2035.09, monoclinic, space group $P2_1/c$, a = 22.9220(10), b = 20.5120(10), c = 20.6540(10) Å, β = 107.733(10)°, V = 9249.6(8) $Å^3$, Z = 4, Mo-K_α radiation, 273(2) K, 23236 reflections, 13209 independent, 1084 parameters, 1006 restraints, R_1 = 0.0697 ($I > 2\sigma$) and wR_2 (all data) = 0.2303.

$Pd_2[(C_6H_4)PPh_2]_2[OSCC_6H_5]_2$ (2b): Compound **2b** was obtained by the reaction of potassium thiobenzoate with $[Pd_2[(C_6H_4)PPh_2]_2(NCMe)_4][BF_4]_2$. The potassium thiobenzoate was prepared by the reaction of a CH_2Cl_2 solution (2 mL) of thiobenzoic acid (31 mg, 0.225 mmol) with potassium hydroxide (13 mg, 0.230 mmol) dissolved in the minimum amount of methanol. This solution was added to $[Pd_2[(C_6H_4)PPh_2]_2(NCMe)_4][BF_4]_2$, which was prepared by the reaction of a suspension of **1** (100 mg, 0.056 mmol) in CH_2Cl_2/NCMe (8:1, 20 mL) with $AgBF_4$ (46 mg, 0.236 mmol). After 5 min of stirring, the solution was evaporated to dryness. The yellow crude product obtained was extracted with dichloromethane, and the solution was filtered through a short plug of Celite and evaporated to dryness. The product was purified by silica gel chromatography with hexane/CH_2Cl_2 (1:1) as the eluent. A yellow solid was obtained by precipitation with hexane and collected by filtration, yield 83.0 mg (73%). ^{1}H NMR ($CDCl_3$, 500 MHz, 298 K): δ = 7.56 (m, 4 H, Ar), 7.49 (m, 4 H, Ar), 7.24 (m, 6 H, Ar), 7.06 (m, 12 H, Ar), 6.92 (m, 2 H, Ar), 6.85 (m, 4 H, Ar), 6.79 (m, 2 H, Ar), 6.61 (m, 4 H, Ar) ppm. ^{31}P NMR ($CDCl_3$, 202 MHz, 298 K): δ = 13.8 (s) ppm. ^{13}C NMR ($CDCl_3$, 125 MHz, 298 K): δ = 210.7 (s, COS) 159.0 (t, $^{3}J_{P,C}$ = 12 Hz, C metalated), 140.6–122.0 (Ar) ppm. $C_{50}H_{38}O_2P_2Pd_2S_2$ (1009.72): calcd. C 59.47, H 3.79; found C 60.04, H 3.95.

X-ray Crystal Structure Data for 2b: Empirical formula $C_{50}H_{38}O_2S_2P_2Pd_2$, M_r = 1009.66, triclinic, space group $P\bar{1}$, a = 14.9440(4), b = 16.2570(4), c = 19.0890(5) Å, α = 91.6990(16), β = 111.1940(12), γ = 93.9340(14)°, V = 4306.30(19) $Å^3$, Z = 4, Mo-K_α radiation, 273(2) K, 27781 reflections, 19043 independent, 1045 parameters, 0 restraints, R_1 = 0.0418 ($I > 2\sigma$) and wR_2 (all data) = 0.1165.

$Pd_2[(C_6H_4)PPh_2]_2[OXCC_6H_5]_2Cl_2$ (X = O, 3a; X = S, 3b): To a solution of **2a** or **2b** (0.040 mmol) in CH_2Cl_2 (5 mL) at 223 K was added iodobenzene dichloride (12 mg, 0.045 mmol). The solution immediately changed from yellow to red. After 5 min of stirring, the solution was evaporated to dryness and hexane was added. The red microcrystalline precipitate obtained was isolated by filtration and washed with hexane, yield 30 mg (72%) **3a**; 39 mg (90%) **3b**.

Characterization Data for 3a: ^{1}H NMR (CD_2Cl_2, 400 MHz, 223 K): δ = 8.16 (m, 6 H, Ar), 7.76 (m, 2 H, Ar), 7.59 (m, 2 H, Ar), 7.46 (m, 6 H, Ar), 7.30 (m, 4 H, Ar), 7.11 (m, 12 H, Ar), 6.96 (m, 4 H, Ar), 6.82 (m, 2 H, Ar) ppm. ^{31}P NMR (CD_2Cl_2, 400 MHz, 223 K): δ = –13.0 (s) ppm. ^{13}C NMR (CD_2Cl_2, 400 MHz, 223 K): δ = 179.5.1 (s, COO), 154.2 (m, C metalated), 145.0.8–124.0 (Ar) ppm. $C_{50}H_{38}Cl_2O_4P_2Pd_2$ (1048.50): calcd. C 57.26, H 3.62; found C 57.52, H 3.45.

X-ray Crystal Structure Data for 3a: Empirical formula $C_{50}H_{38}O_4Cl_2P_2Pd_2{\cdot}4O(H_2)$, M_r = 1114.46, monoclinic, space group $C2/c$, a = 15.0680(7), b = 17.6230(8), c = 20.1580(6) Å, β = 107.235(2)°, V = 5112.5 (4) $Å^3$, Z = 4, Mo-K_α radiation, 273(2) K, 9757 reflections, 5825 independent, 284 parameters, 0 restraints, R_1 = 0.0550 ($I > 2\sigma$) and wR_2 (all data) = 0.1869.

Characterization Data for 3b: ^{1}H NMR (CD_2Cl_2, 400 MHz, 223 K): δ = 8.11 (m, 4 H, Ar), 7.66 (m, 6 H, Ar), 7.55 (m, 4 H,

Ar), 7.35 (m, 4 H, Ar), 7.12 (m, 6 H, Ar), 7.03 (m, 8 H, Ar), 6.87 (m, 4 H, Ar), 6.77 (m, 2 H, Ar) ppm. ^{31}P NMR (CD_2Cl_2, 400 MHz, 223 K): δ = –16.9 (s) ppm. ^{13}C NMR (CD_2Cl_2, 400 MHz, 223 K): δ = 212.9 (s, COS), 154.7 (m, C metalated), 145.4–124.0 (Ar) ppm.

Acetoxylation of 2-Phenylpyridine: 2-Phenylpyridine (60 μL, 0.33 mmol), $PhI(OAc)_2$ (326 mg, 1 mmol), and catalyst (**2a** or **2b**, 0.015 mmol) were mixed in solvent (2.2 mL), and the solution was heated at the indicated temperature and time. The solvent was removed under vacuum, and the resulting solid was purified by silica gel column chromatography with hexanes/ethyl acetate (90:10) as the eluent.

Compound 5: ^{1}H NMR ($CDCl_3$, 400 MHz, 298 K): δ = 8.77 (ddd, $J_{H,H}$ = 6.0, $J_{H,H}$ = 1.8, $J_{H,H}$ = 1.0 Hz, 1 H), 7.85 (m, 1 H), 7.71 (dd, $J_{H,H}$ = 7.6, $J_{H,H}$ = 2.0 Hz, 1 H), 7.59 (m, 1 H), 7.46 (m, 1 H), 7.38 (dd, $J_{H,H}$ = 7.6, $J_{H,H}$ = 1.3 Hz, 1 H), 7.34 (m, 1 H), 7.20 (dd, $J_{H,H}$ = 8.0, $J_{H,H}$ = 1.3 Hz, 1 H), 2.18 (s, 3 H, CH_3) ppm. ^{13}C NMR ($CDCl_3$, 100 MHz): δ = 169.3 (s, $C_{quat.}$), 154.9 (s, $C_{quat.}$), 148.6 (s, CH), 148.0 (s, $C_{quat.}$), 137.5 (s, CH), 131.8 (s, $C_{quat.}$), 130.9 (s, CH), 130.2 (s, CH), 126.5 (s, CH), 124.2 (s, CH), 123.2 (s, CH), 122.6 (s, CH), 20.9 (s, CH_3) ppm.

Direct Catalytic Phenylation of 1-Methylindole and Indole: The procedure reported by Sanford and co-workers was followed.[10] 1-Methylindole (**6a**) or indole (**6b**; 58.6 mg, 0.5 mmol), and the precatalyst **2a** or **2b** (0.0125 mmol, 2.5 mol-% of Pd) were dissolved in CH_3CO_2H (5 mL), and the solution was stirred at 298 K for 5 min. $[Ph_2I]PF_6$ (426.0 mg, 1 mmol) was added, and the resulting solution was stirred at 298 K. The reaction mixture was filtered through a plug of siliceous earth, and the solvents were evaporated to dryness. The resulting oil was dissolved in CH_2Cl_2 (25 mL) and extracted with aqueous $NaHCO_3$ (2 × 40 mL). The organic phase was dried with Na_2SO_4 and concentrated, and the product was purified by silica gel chromatography with hexanes/ethyl acetate (96:4) as the eluent.

Compound 8a: ^{1}H NMR ($CDCl_3$, 400 MHz): δ = 7.75 (d, $^3J_{H,H}$ = 7.6 Hz, 1 H), 7.63–7.60 (m, 2 H), 7.56 (t, $^3J_{H,H}$ = 7.6 Hz, 2 H), 7.51–7.45 (m, 2 H), 7.36 (dt, $^3J_{H,H}$ = 8.0, $^3J_{H,H}$ = 1.2 Hz, 1 H), 7.26 (m, 1 H), 6.68 (s, 1 H), 3.83 (s, 3 H, CH_3) ppm. ^{13}C NMR ($CDCl_3$, 100 MHz): δ = 141.7 (s, $C_{quat.}$), 138.5 (s, $C_{quat.}$), 132.9 (s, $C_{quat.}$), 129.5 (s, 2 CH), 128.6 (s, 2 CH), 128.1 (s, $C_{quat.}$), 127.9 (s, CH), 121.8 (s, CH), 120.6 (s, CH), 120.0 (s, CH), 109.7 (s, CH), 101.8 (s, CH), 31.2 (s, CH_3) ppm.

Compound 8b: ^{1}H NMR ($CDCl_3$, 400 MHz): δ = 8.31 (br s, 1 H), 7.69–7.65 (m, 3 H), 7.49–7.39 (m, 3 H), 7.356 (t, $^3J_{H,H}$ = 7.4 Hz, 1 H), 7.23 (ddd, $^3J_{H,H}$ = 7.8, $^3J_{H,H}$ = 7.0, $^3J_{H,H}$ = 1.2 Hz, 1 H), 7.16 (ddd, $^3J_{H,H}$ = 7.7, $^3J_{H,H}$ = 7.0, $^3J_{H,H}$ = 1.0 Hz, 1 H), 6.86 (s, 1 H) ppm. ^{13}C NMR ($CDCl_3$, 100 MHz): δ = 137.8 (s, $C_{quat.}$), 136.7 (s, $C_{quat.}$), 132.2 (s, $C_{quat.}$), 129.2 (s, 2 CH), 129.0 (s, 2 CH), 127.7 (s, $C_{quat.}$), 125.1 (s, CH), 122.3 (s, CH), 120.6 (s, CH), 120.2 (s, CH), 110.9 (s CH), 99.9 (s, CH) ppm.

Computational Details: All models were fully optimized with the Gaussian09 program package[23] at the DFT level of theory. The hybrid density functional B3PW91[24,25] was utilized together with a basis set consisting of the Stuttgart–Dresden effective core potential basis set with an additional p-polarization function for Pd atoms [SDD(p)] and the standard all-electron basis set 6-31G(d) for all other atoms. Frequency calculations with no scaling were conducted to ensure optimization to true minima. None of the optimized structures gave imaginary frequencies.

Topological charge-density analysis was performed by the QTAIM[26] method, which allowed us to access the nature of the bonding through the calculation of different properties of the electron density at the BCPs. The analysis was done with the AIMALL program[27] by using the wavefunctions obtained from the DFT calculations with the computationally optimized structures.

Acknowledgments

The authors are grateful to Servei Central de Suport a la Investigació Experimental (SCSIE) of the Universitat de València for instrumental support. Financial support provided by the Inorganic Materials Chemistry Graduate Program (EMTKO) and the strategic funding of the University of Eastern Finland is gratefully acknowledged (grant to A. O.). The computational work has been facilitated by the use of the Finnish Grid Infrastructure resources.

[1] a) D. C. Powers, T. Ritter, *Top. Organomet. Chem.* **2011**, *35*, 129–156; b) L. M. Mirica, J. R. Khusnutdinova, *Coord. Chem. Rev.* **2013**, *257*, 299–314.
[2] F. A. Cotton, J. Gu, C. A. Murillo, D. J. Timmons, *J. Am. Chem. Soc.* **1998**, *120*, 13280–13281.
[3] a) F. A. Cotton, I. O. Koshevoy, P. Lahuerta, C. A. Murillo, M. Sanaú, M. A. Úbeda, Q. Zhao, *J. Am. Chem. Soc.* **2006**, *128*, 13674–13679; b) D. Penno, V. Lillo, I. O. Koshevoy, M. Sanaú, M. A. Úbeda, P. Lahuerta, E. Fernández, *Chem. Eur. J.* **2008**, *14*, 10648–10655; c) D. Penno, E. Estevan, F. Fernández, P. Hirva, P. Lahuerta, M. Sanaú, M. A. Úbeda, *Organometallics* **2011**, *30*, 2083–2094; d) S. Ibañez, F. Estevan, P. Hirva, M. Sanaú, M. A. Úbeda, *Organometallics* **2012**, *31*, 8098–8108; e) S. Ibañez, D. N. Vrečko, F. Estevan, P. Hirva, M. Sanaú, M. A. Úbeda, *Dalton Trans.* **2014**, *43*, 2961–2970; f) S. Ibañez, L. Oresmaa, F. Estevan, P. Hirva, M. Sanaú, M. A. Úbeda, *Organometallics* **2014**, *33*, 5378–5391.
[4] a) D. C. Powers, T. Ritter, *Nature* **2009**, *1*, 302–309; b) D. C. Powers, M. A. L. Geibel, J. E. M. N. Kein, T. Ritter, *J. Am. Chem. Soc.* **2009**, *131*, 17050–17051; c) G. J. Chuang, W. Wang, E. Lee, T. Ritter, *J. Am. Chem. Soc.* **2011**, *133*, 1760–1762.
[5] M. G. Campbell, D. C. Powers, J. Raynaus, M. J. Graham, P. Xie, E. Lee, T. Ritter, *Nature Chem.* **2011**, *3*, 949–953.
[6] D. C. Powers, T. Ritter, *Organometallics* **2013**, *32*, 2042–2045.
[7] a) J. R. Khusnutdinova, N. P. Rath, L. M. Mirica, *Angew. Chem. Int. Ed.* **2011**, *50*, 5532–5536; b) S. E. Eitel, M. Bauer, D. Schweinfurth, N. Deibel, B. Sarkar, H. Kelm, H.-J. Krüger, W. Frey, R. Peters, *J. Am. Chem. Soc.* **2012**, *134*, 4683–4693.
[8] a) A. J. Canty, A. Ariafard, M. S. Sanford, B. F. Yates, *Organometallics* **2013**, *32*, 544–555; b) J. Le Bras, J. Muzard, *Chem. Rev.* **2011**, *111*, 1170–1214; c) T. Yoneyama, R. H. Crabtree, *J. Mol. Catal. A* **1996**, *108*, 35–40; d) L. M. Stock, K.-t. Tse, L. J. Vorvick, S. A. Walstrum, *J. Org. Chem.* **1981**, *46*, 1757–1759.
[9] N. R. Deprez, M. S. Sanford, *Inorg. Chem.* **2007**, *46*, 1924–1935.
[10] A. J. Hickman, M. S. Sanford, *Nature* **2012**, *484*, 177–185.
[11] a) D. C. Powers, D. Benitez, E. Tkatchouk, W. A. Goddard, T. Ritter, *J. Am. Chem. Soc.* **2010**, *132*, 14092–14103; b) D. C. Powers, D. Y. Xiao, M. A. L. Geibel, T. Ritter, *J. Am. Chem. Soc.* **2010**, *132*, 14530–14536; c) D. C. Powers, T. Ritter, *Acc. Chem. Res.* **2012**, *45*, 840–850.
[12] J. R. Khusnutdinova, N. P. Rath, L. M. Mirica, *Angew. Chem. Int. Ed.* **2011**, *50*, 5532–5536.
[13] S. R. Neufeld, M. S. Sanford, *Acc. Chem. Res.* **2012**, *45*, 936–946.
[14] A. R. Dick, K. L. Hull, M. S. Sanford, *J. Am. Chem. Soc.* **2004**, *126*, 2300–2301.
[15] N. R. Deprez, D. Kalyani, A. Krause, M. S. Sanford, *J. Am. Chem. Soc.* **2006**, *128*, 4972–4973.
[16] I. O. Koshevoy, P. Lahuerta, M. Sanaú, M. A. Úbeda, A. Domenech, *Dalton Trans.* **2006**, 5536–5541.
[17] a) I. V. Umakoshi, A. Ichimura, I. Kinoshita, S. Ooi, *Inorg. Chem.* **1990**, *29*, 4005–4010; b) A. C. Durrell, M. N. Jackson, N. Hazari, H. B. Gray, *Eur. J. Inorg. Chem.* **2013**, 1134–1137.

[18] D. Kalyani, M. S. Sanford, *Org. Lett.* **2005**, *7*, 4149–4152.
[19] D. V. Davidson, S. K. Garg, *Can. J. Chem.* **1972**, *50*, 3515–3520.
[20] a) F. Estevan, A. García-Bernabé, P. Lahuerta, M. Sanaú, M. A. Úbeda, M. C. Ramírez de Arellano, *Inorg. Chem.* **2000**, *30*, 5964–5969; b) A. M. Aarif, F. Estevan, A. García-Bernabé, P. Lahuerta, M. Sanaú, M. A. Úbeda, *Inorg. Chem.* **1997**, *36*, 6472–6475.
[21] H. J. Lucas, E. R. Kennedy, *Org. Synth. Coll. Vol. III*, John Wiley & Sons, New York, **1955**, p. 482.
[22] *SHELXTL*, version 6.14, Bruker, AXS Inc., Madison, Wisconsin, USA, **2000**.
[23] M. J. Frisch, G. W. Trucks, H. B. Schlegel, G. E. Scuseria, M. A. Robb, J. R. Cheeseman, G. Scalmani, V. Barone, B. Mennucci, G. A. Petersson, H. Nakatsuji, M. Caricato, X. Li, H. P. Hratchian, A. F. Izmaylov, J. Bloino, G. Zheng, J. L. Sonnenberg, M. Hada, M. Ehara, K. Toyota, R. Fukuda, J. Hasegawa, M. Ishida, T. Nakajima, Y. Honda, O. Kitao, H. Nakai, T. Vreven, J. A. Montgomery Jr., J. E. Peralta, F. Ogliaro, M. Bearpark, J. J. Heyd, E. Brothers, K. N. Kudin, V. N. Staroverov, R. Kobayashi, J. Normand, K. Raghavachari, A. Rendell, J. C. Burant, S. S. Iyengar, J. Tomasi, M. Cossi, N. Rega, J. M. Millam, M. Klene, J. E. Knox, J. B. Cross, V. Bakken, C. Adamo, J. Jaramillo, R. Gomperts, R. E. Stratmann, O. Yazyev, A. J. Austin, R. Cammi, C. Pomelli, J. W. Ochterski, R. L. Martin, K. Morokuma, V. G. Zakrzewski, G. A. Voth, P. Salvador, J. J. Dannenberg, S. Dapprich, A. D. Daniels, O. Farkas, J. B. Foresman, J. V. Ortiz, J. Cioslowski, D. J. Fox, *Gaussian 09*, revision C.01, Gaussian, Inc., Wallingford CT, **2009**.
[24] A. D. Becke, *J. Chem. Phys.* **1993**, *98*, 5648–5652.
[25] J. P. Perdew, Y. Wang, *Phys. Rev. B* **1992**, *45*, 13244–13249.
[26] R. F. W. Bader, *Atoms in Molecules: A Quantum Theory*, Clarendon Press, Oxford, UK, **1990**.
[27] *AIMAll*, version 12.06.03, Todd A. Keith, TK Gristmill Software, Overland Park KS, USA, **2012** (aim.tkgristmill.com).

Received: March 25, 2015
Published Online: May 27, 2015

